Supplementary information

Structure-based discovery of small molecules that allosterically modulate RNA function

Zhiling Pan[1,2]†, Hao Wu[3,4]†, Han Hu[5,]†, Jian Zou[2,]†, Haiyun Ma[2,]†, Hongshan Ni[6,]†, Liu Wang[7], Jiaqi Zhao[5], Xiaoqi Sun,[8,9], Jiayu Dong[8], Sheng Xu[3,4], Yu Cheng[10], Ling Liu[8,]*, Ke Zheng[6,]*, Siqi Sun[3,4,]*, Zhaoming Su[2,]*

[1]School of Pharmacy, Chengdu University, Chengdu, 610051, China.
[2]State Key Laboratory of Biotherapy, West China Hospital, Sichuan University, Chengdu, 610044, China.
[3]Research Institute of Intelligent Complex Systems, Fudan University, Shanghai, 200437, China.
[4]Shanghai Artificial Intelligence Laboratory, Shanghai, 200030, China.
[5]Mingle Scope (Chengdu), 138 2nd Tianfu Street, Chengdu, 610096, China.
[6]Key Laboratory of Green Chemistry & Technology, Ministry of Education, College of Chemistry, Sichuan University, Chengdu 610064, China.
[7]State Key Laboratory of Oral Diseases, National Clinical Research Center for Oral Diseases, National Center for Stomatology, Department of Cariology and Endodontics, West China Hospital of Stomatology, Sichuan University, Chengdu, 610044, China.
[8]State Key Laboratory of Microbial Diversity and Innovative Utilization, Institute of Microbiology, Chinese Academy of Sciences, University of Chinese Academy of Sciences, Beijing 100101, China.
[9]School of Biomedical Sciences, Shandong First Medical University & Shandong Academy of Medical Sciences, Jinan 250117, China.
[10]Department of Computer Science and Engineering, The Chinese University of Hong Kong, Hong Kong 999077, China.

†These authors contributed equally.
*Correspondence should be addressed to Z.S. (zsu@wchscu.cn), S.S. (siqisun@fudan.edu.cn), K.Z. (kzheng@scu.edu.cn), and L.L. (liul@im.ac.cn).

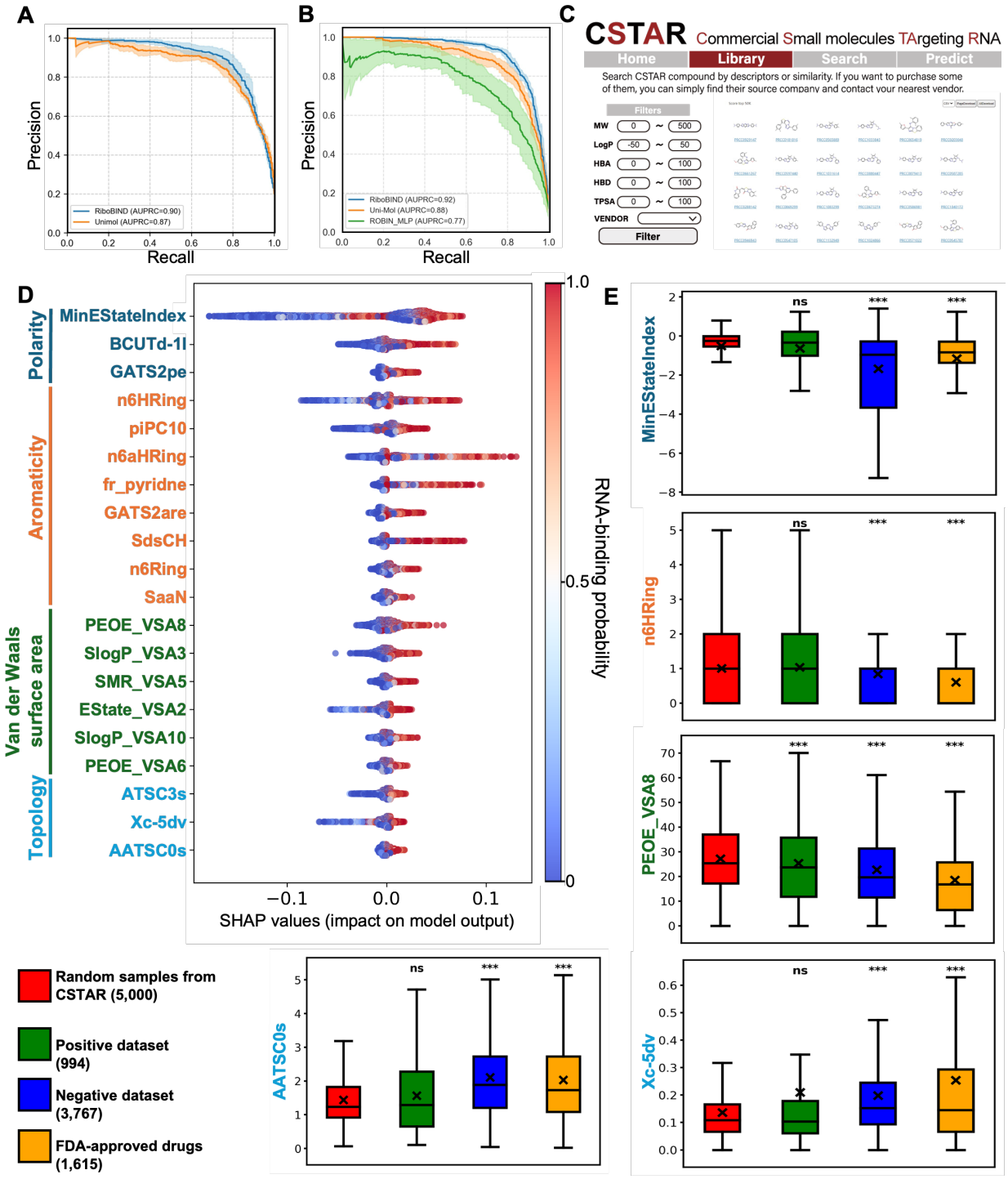

Figure S1 | Curation of CSTAR library and analysis of RNA-binding propensities, related to Fig. 1. A, Comparison of AUPRC curves between RiboBIND and Uni-MOL on CSTAR benchmark dataset. **B,** Comparison of AUPRC curves among RiboBIND, Uni-MOL and ROBIN MLP model on ROBIN benchmark dataset. **C,** CSTAR website snapshot. **D,** Beeswarm plot illustrating 20 most impactful descriptors to the SHAP model, most of which could explicitly separate RNA-binding (red) from protein-binding (blue). The descriptors were divided into four

major category, including polarity, aromaticity, Van der Waals surface area and topology. **E,** Comparisons using box and whisker plots of five representative descriptors among four datasets, including 5,000 compounds randomly sampled from the CSTAR library (red), 994 compounds from the positive dataset (green), 3,767 compounds from the negative dataset (blue), and 1,615 FDA-approved drugs (yellow). The whiskers represent 10-90% of data with outliers excluded, and the boxes contain the middle 50% of the data. The black lines and × signs denote the medians and means, respectively. Descriptros of MinEstateIndex (Minimum E-state value), n6HRing (Number of 6-membered heterorings), PEOE_VSA8 (Van der Waals surface area with partial charges range from 0.20-0.25), Xc-5dv(5th-order valence connectivity index), and AATSC0s (Average E-state value for carbon atoms at zero topological distance) were selected. T-tests were performed between the CSTAR representatives and three other datasets. ns, $P>0.05$; *, $P\leq0.05$; **, $P\leq0.01$; ***, $P\leq0.001$.

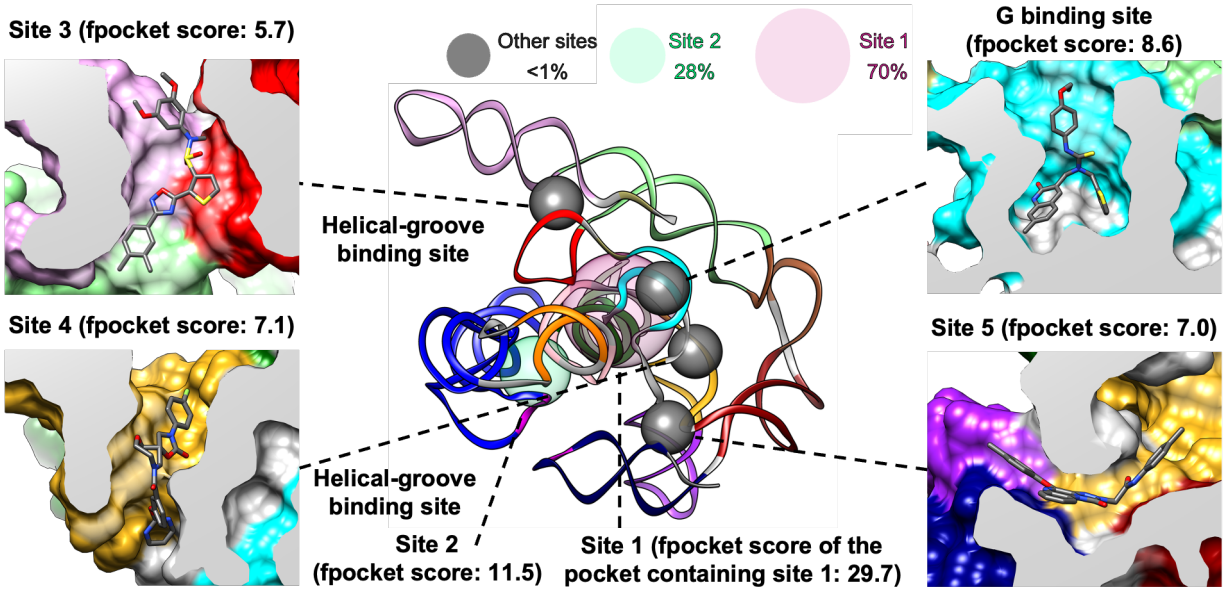

Figure S2 | The remaining binding sites identified from molecular docking of 8,392 diversified CSTAR compounds, related to Fig. 2. The two major sites 1 (transparent violet red) and 2 (transparent spring green) contained ~98% of the docked small molecules with scores of -50 and lower, and the pocket scores were 29.7 for site 1 (a pocket ~2.5 times larger in volume than site 2) and 11.5 for site 2, as determined by fpocket. The remaining site 3, 4, 5 and G-binding site were shown in grey, with pocket scores of 5.7, 7.1, 7.0 and 8.6, respectively. Representative small molecules for each site were shown in the molecular surfaces colored according to the model.

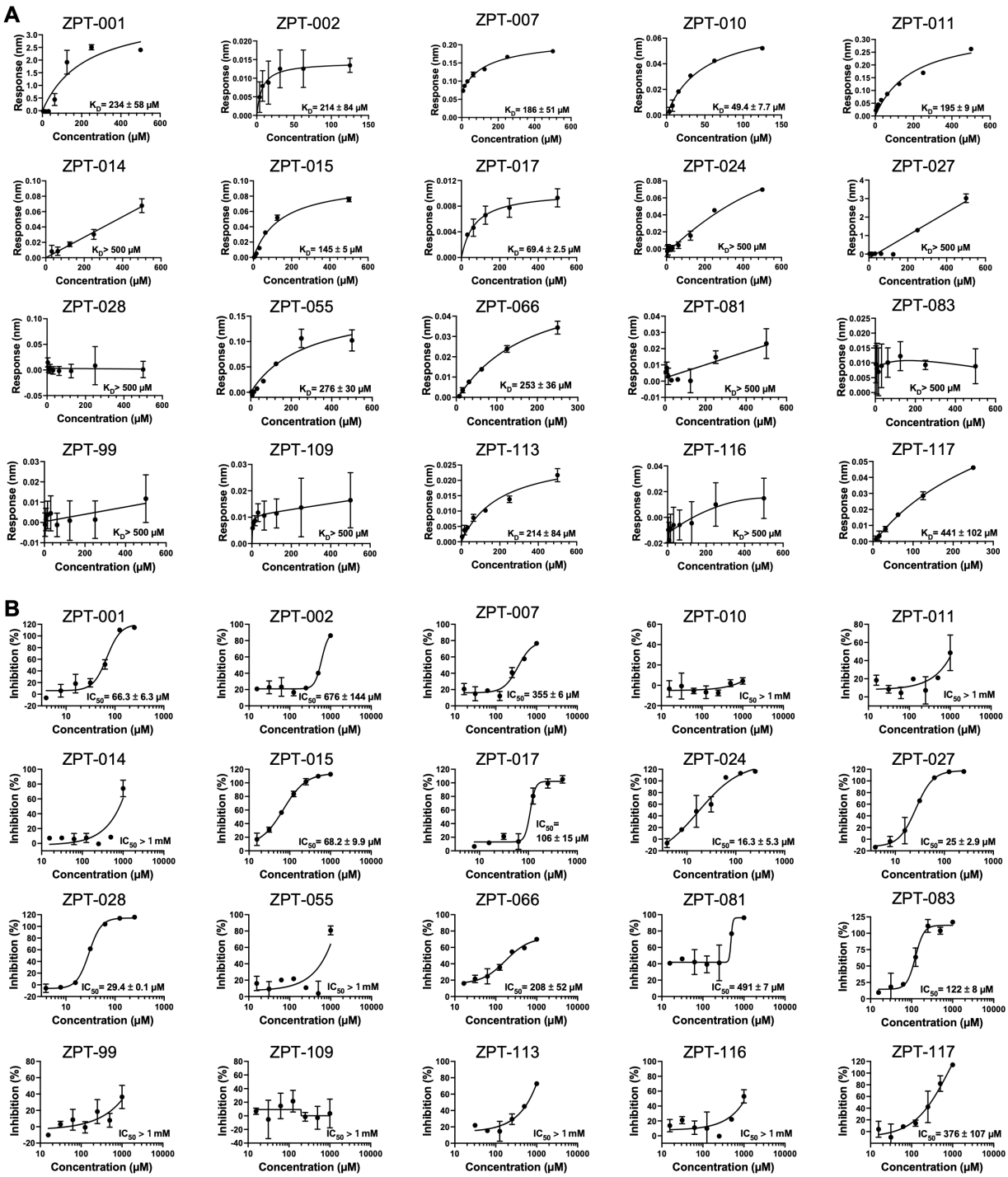

Figure S3 | Binding affinity and inhibition activity curves of selected compounds, related to Fig. 3. A, Binding affinity curves for 20 compounds selected from preliminary screening. **B,** Dose-response curves for catalysis inhibition of 20 compounds selected from preliminary screening. All data were presented as mean values ± standard deviation (SD) from two independent experiments.

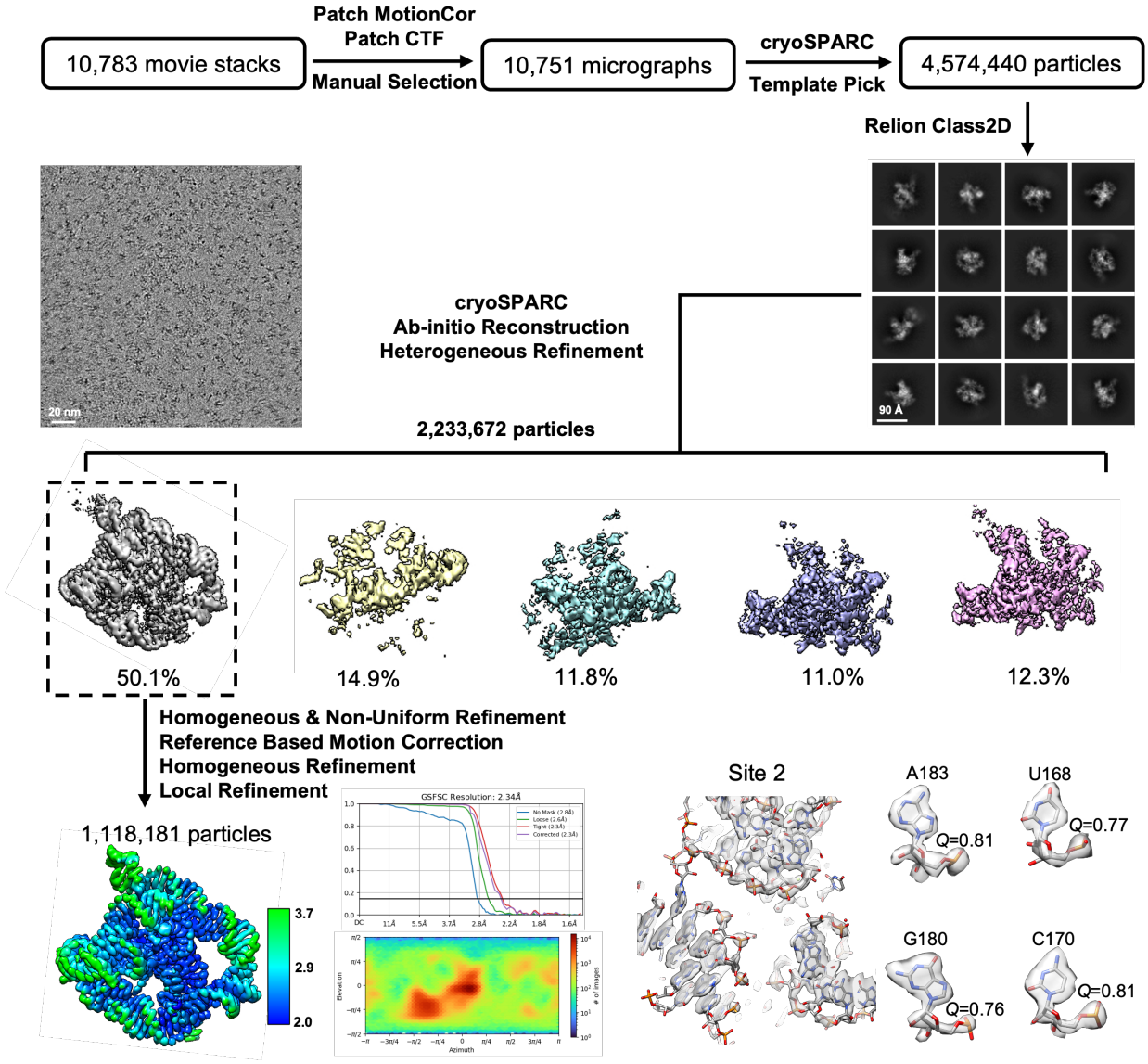

Figure S4 | Cryo-EM data processing of L-16 in complex with ZPT-005, related to Fig. 4. The cryo-EM processing workflow including representative micrograph, 2D classification, 3D classification, 3D reconstruction, FSC curve and particle orientation distribution. Cryo-EM map and model surrounding site 2 were presented.

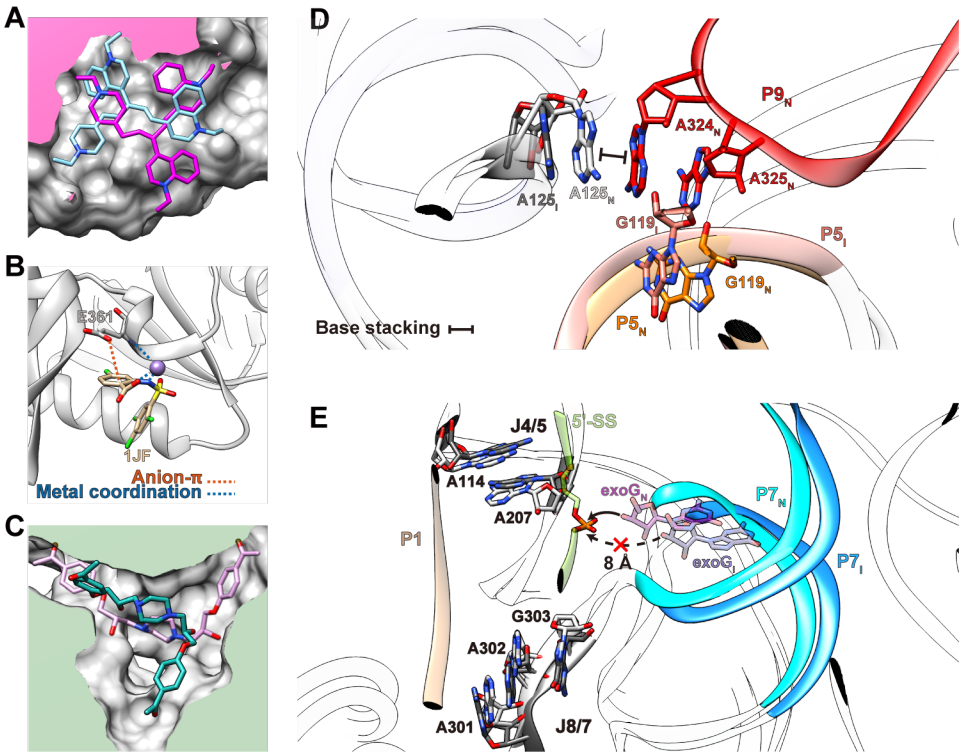

Figure S5 ZPT-005 and ZPT-084 recognition patterns and MOAs, related to Fig. 4 and 5. **A,** Comparison of experimental (magenta) and docked (light blue) ZPT-005 conformations. **B,** The anion-π and metal coordination interactions previously reported in a HCV NS5B polymerase inhibitor (PDB 4J04). **C**, Comparison of experimental (light sea green) and docked ZPT-084 (pink) conformations. **D,** Conformational change of P5 (orange) and J5/5a (grey) disrupted hydrogen bonds and stacking of P5/L9 (red) tertiary interaction. **E,** Alignment of P1 docking register residues (grey) between N and I conformations revealed translocation of G-binding site and exoG 8 Å away from the 5'-SS to inhibit catalysis.

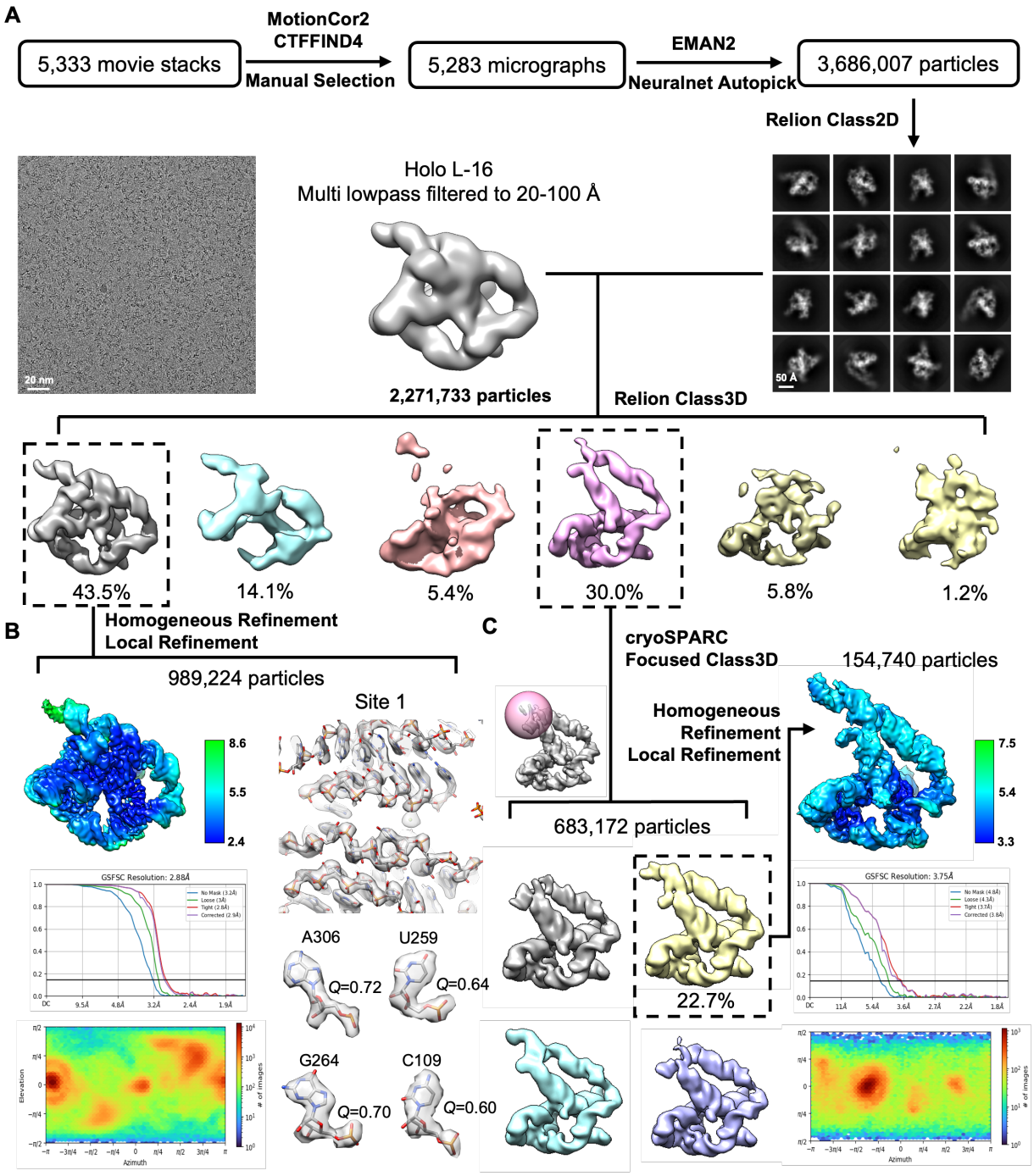

Figure S6 | Cryo-EM data processing of L-16 in complex with ZPT-084, related to Fig. 5. A, The cryo-EM processing workflow including representative micrograph, 2D classification and 3D classification, which revealed two different conformations. **B,** Reconstruction of the N conformation at 2.9 Å resolution, with FSC curve and particle orientation distribution. Cryo-EM map and model surrounding site 2 were presented. **C,** Focused classification on P9 and P9.2 of the I conformation resulted a density map at 3.8 Å resolution, with FSC curve and particle orientation distribution.

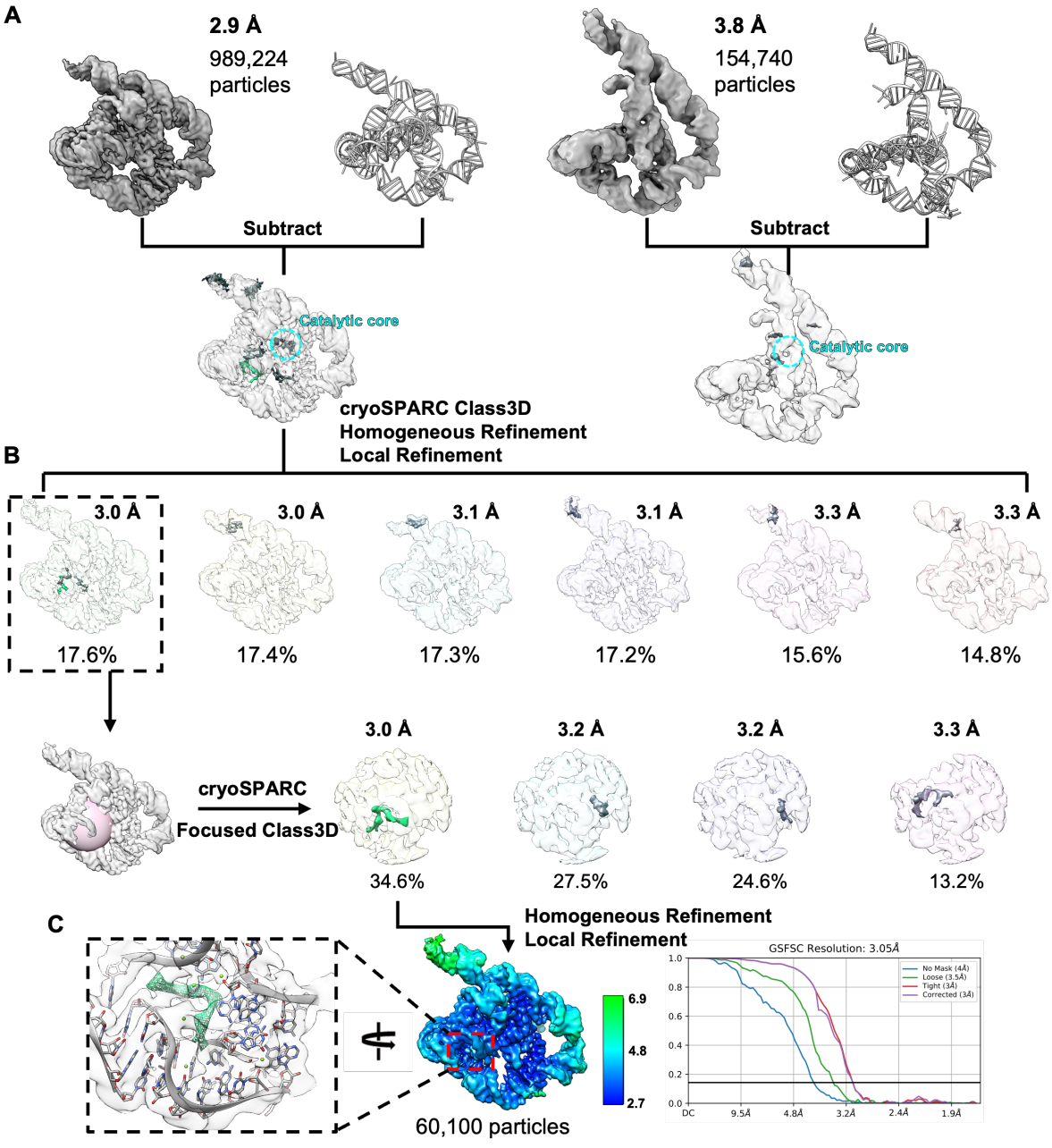

Figure S7 | 3D classification and reconstruction yielded the cryo-EM structure with ZPT-084 density, related to Fig. 5. A, Subtraction of the apo native L-16 model from the ZPT-084 native L-16 density resulted in additional densities in the core region and P9.2 (colored in grey and spring green). Whereas no additional densities were observed in the L-16 I conformation. **B,** 3D classification in cryoSPARC yielded a major class with extra densities in the core regions, whereas the remaining classes contained extra densities in P9.2. Focused 3D classification resulted in a major class with continuous extra density in site 2. **C,** Subsequent refinement yielded the final reconstruction with ZPT-084 density at 3.0 Å resolution.

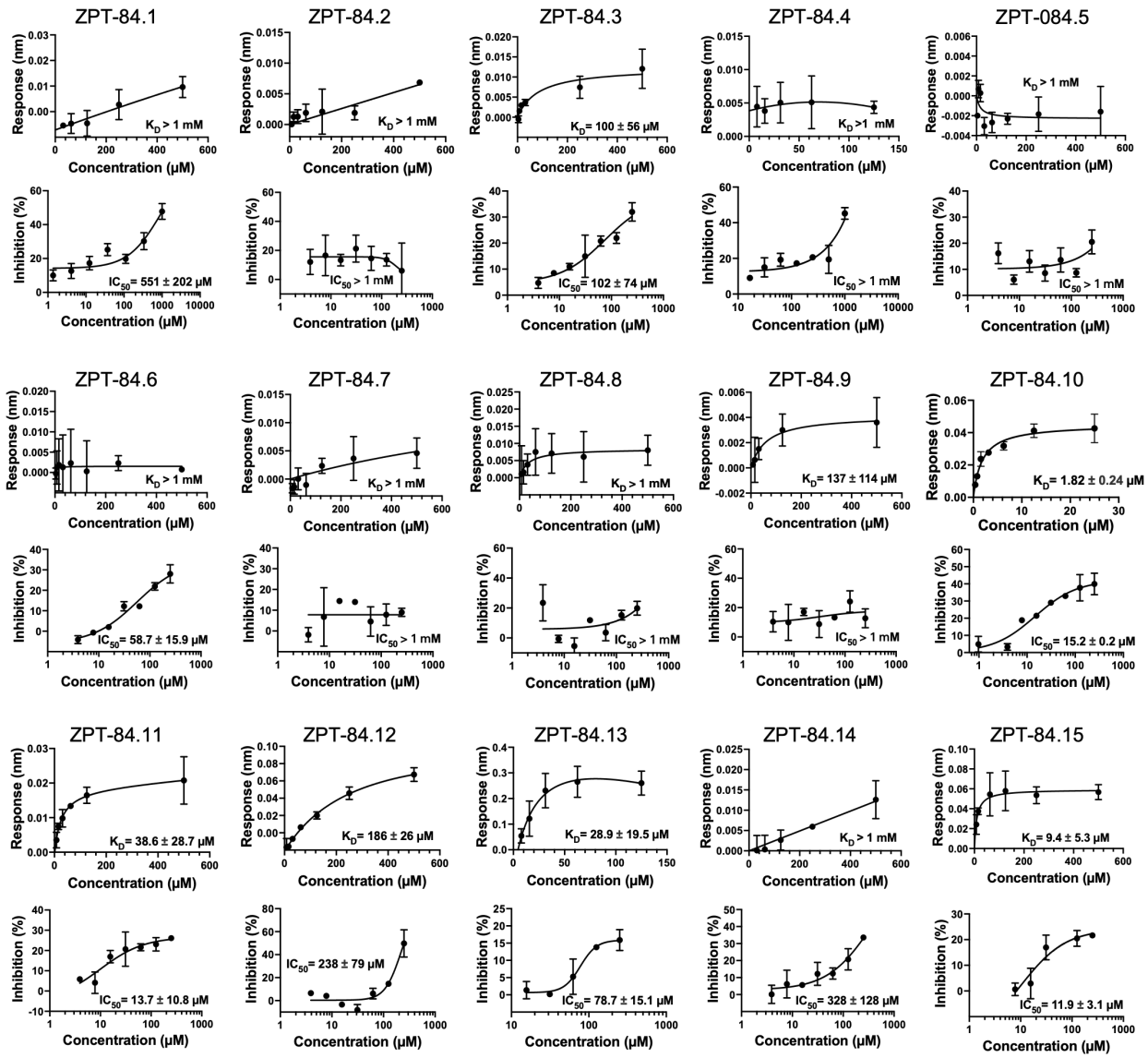

Figure S8| Binding affinity and inhibition activity curves of ZPT-084 optimized compounds, related to Fig. 6. All data were presented as mean values ± standard deviation (SD)

from two independent experiments.

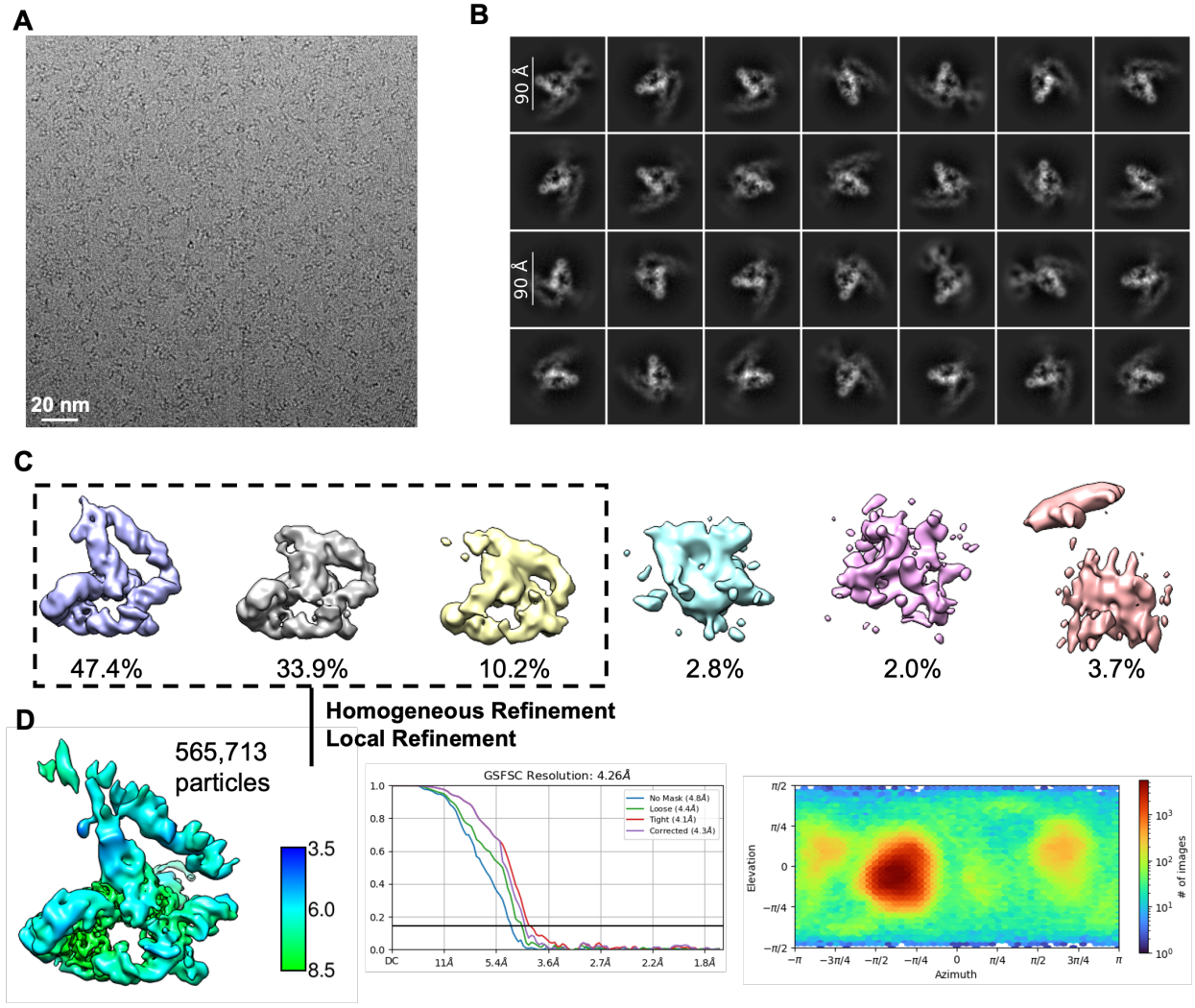

Figure S9 | Cryo-EM data processing of L-16 in complex with ZPT-084.10, related to Fig. 6. **A**, Representative cryo-EM micrograph of L-16 in complex with ZPT-084.10. **B**, Representative 2D class averages showing predominant L-16 in I conformation. **C**, 3D classification showing predominant population of L-16 in I conformation. **D**, Reconstruction of the L-16 I conformation at 4.3 Å resolution, with FSC curve and particle orientation distribution.

Table S1. Cryo-EM data collection, processing, and model refinement statistics.

Cryo-EM data collection and processing	**L-16-ZPT-005 (9UTI)**	**L-16-ZPT-084**	
		N state (9J9X)	**I state (9JC8)**
Microscope	Titan Krios G4	Titan Krios G3i	
Voltage (kV)	300		
GIF Quantum energy filter slit width (eV)	10	20	
Detector	Falcon 4i	Gatan K2	
Nominal Magnification			
Pixel size (Å)	0.74	0.85	
Symmetry imposed			
Defocus range (μm)	-0.7 to -1.1	-1.2 to -2.0	
Electron exposure ($e^-/Å^2$)	48	60	
Micrographs (acquired/used)	10,783/10,751	5,333/5,283	
Number of extracted particles	4,574,440	3,686,007	
Number of particles after 2D classifications	2,233,672	2,271,733	
Number of particles going to 3D refinement	1,118,181	60,100	154,740
Map resolution at 0.143 FSC criterion (Å)	2.3	3.0	3.8
Local resolution range (Å)	2.0-4.0	2.7-6.9	3.3-7.5
Sharpening B-factor ($Å^2$)	-91	-90	-200
Model refinement			
Atoms	8,705	8,235	8,202
Residues	382	382	382
CC_{mask}	0.72	0.73	0.67
$Resolution_{FSC\ map\ vs.\ model\ @\ 0.5}$ (Å)	2.7	3.3	3.8
Root mean aquare deviation			
Bond lengths (Å)	0.003	0.003	0.003
Bond angles (°)	0.747	0.689	0.814
Validation			
Clash score	2.0	2.5	4.4
MolProbity score	1.8	2.2	2.4

Table S2. Metal ions identified in the cryo-EM structures of L-16 in complex with ZPT-005, in addition to those previously reported in previous studies.

Metal	Region	Coordinate	Metal	Region	Coordinate
M_4	P5a A-rich bulge	$2H_2O$-A184 OP1-A186 OP1-A187 OP2-G188 OP2	M_{64}	J8/7	H_2O-U300 OP2
M_5	P5a A-rich bulge	$3H_2O$-A183 OP1-A184 OP2-A186 OP2	M_{65}	J8/7	A304 OP2
M_6	P5a A-rich bulge	$5H_2O$-G188 O6	M_{66}	J8/7	A304 OP2-U305 O2'
M_{11}	Between P3 and P6	$4H_2O$-A256 OP1-U273 OP1	M_{67}	P3 major groove	G96 N7
M_{16}	Between P6 and J6a/6	$5H_2O$-U258 OP1	M_{68}	J8/7	H_2O-G303 OP1
M_{19}	J8/7	$4H_2O$-A301 OP2-A302 OP1	M_{69}	Between P3 and P6a	H_2O-A256 N6-U273 OP2
M_{26}	Between P4 and J8/7	$3H_2O$-C208 OP1-A304 OP1-A306 OP2	M_{70}	P4 major groove	G112 N7
M_{35}	P5b major groove	A140 O2'	M_{71}	J3/4	A105 OP1-U106 OP2
M_{36}	P5a major groove	A183 O2'-G188 OP1	M_{72}	P8 major groove	C298 OP2-A299 OP2
M_{37}	Between P4 and P5b	A214 O3'-G215 OP1-A140 O2'	M_{73}	P5a major groove	A136 O2'-A136 N3
M_{38}	Between P4 and P5a	U185 OP1-C213 O2'	M_{74}	P3 major groove	H_2O-C274 OP2
M_{39}	P5a major groove	U185 OP2-U185 O2'	M_{75}	P8 major groove	H_2O-A299 N7
M_{40}	P5a major groove	A187 O2'-G188 OP1	M_{76}	P8 major groove	A299 O2’
M_{41}	P4 major groove	C211 OP1	M_{77}	Between J3/4 and P7	$2H_2O$-A104 OP2-U267 OP2
M_{42}	P4 major groove	H_2O-C213 OP2	M_{78}	P2 major groove	A46 OP2
M_{43}	P4 major groove	A214 OP2	M_{79}	Between P7 and P9a	A314 OP1-C316 N4
M_{44}	P6a major groove	G254 OP1-C255 OP2	M_{80}	P9 major groove	G328 OP2
M_{45}	P6a major groove	$2H_2O$-C255 O2'-G257 OP2	M_{81}	P6 major groove	A248 OP2
M_{46}	P6a major groove	C255 OP1	M_{82}	P4 major groove	G111 OP1-G112 OP2
M_{47}	P5c major groove	H_2O-G164 OP1	M_{83}	P2 major groove	U36 O2 U36 O2’
M_{48}	P5c major groove	H_2O-C165 OP2-U167 O2'	M_{84}	P7 major groove	A265 OP2-C266 OP2
M_{49}	Beween P5a and P5b	G164 N7-G180 N2	M_{85}	Between P7 and P9.1a	U310 O2'-G341 O2'
M_{50}	P5a major groove	H_2O-C138 O2'-A178 N1	M_{86}	P7 major groove	H_2O-A308 N7

M_{51}	P5 major groove	U205 OP2-A206 N7	M_{87}	P14 major groove	C170 OP2-A171 N6
M_{52}	P5 major groove	207 OP1	M_{88}	Between P3 and P7	A103 O2'-A269 N7
M_{53}	Between J3/4 and P4	H_2O-U106 O2'-U107 OP2	M_{89}	P5a major groove	U133 OP1
M_{54}	Between P4 and J6/7	H_2O-G108 N7-U259 O2'	M_{90}	P2 major groove	G32 N7-G32 OP2
M_{55}	Between J6/7 and J8/7	H_2O-C260 OP1-U305 O4	M_{91}	P2 major groove	U56 O4
M_{56}	Between J6/7 and P7	A261 OP1 G264 OP1	M_{92}	P7 major groove	A263 N3-G313 O2'
M_{57}	Between P7 and J8/7	C262 OP1-U305 O2'-A306 OP1	M_{93}	P6a major groove	H2O-U224 O4
M_{58}	Between P3 and P7	H_2O-U271 O4	M_{94}	P9 major groove	U326 O4
M_{59}	Between P3 and P7	U271 OP2	M_{95}	P3 major groove	U277 O2-U277 O2’
M_{60}	P3 major groove	U101 O4-G272 O6	M_{96}	J3/4	A104 OP2-A105 OP2-A105 N7-U106 O4
M_{61}	P3 major groove	H_2O-C274 OP1-G275 OP2	M_{97}	J3/4	A103 OP1
M_{62}	P3 major groove	G275 O2’	M_{98}	P5b major groove	U155 O2’
M_{63}	Between P3 and J8/7	A97 OP2-U300 O2’-A301 OP1	M_{99}	P5b major groove	C154 OP2

115
116

Table S3. RNA and primer sequences in this study.

	Sequence
L-16	5'-UUUGGAGGGGAAAAGUUAUCAGGCAUGCACCUGGUAGCUAGUCUUUAAACC AAUAGAUUGCAUCGGUUUAAAAGGCAAGACCGUCAAAUUGCGGGAAAGGGGU CAACAGCCGUUCAGUACCAAGUCUCAGGGGAAACUUUGAGAUGGCCUUGCAA AGGGUAUGGUAAUAAGCUGACGGACAUGGUCCUAACCACGCAGCCAAGUCCU AAGUCAACAGAUCUUCUGUUGAUAUGGAUGCAGUUCACAGACUAAAUGUCGG UCGGGGAAGAUGUAUUCUUCUCAUAAGAUAUAGUCGGACCUCUCCUUAAUGG GAGCUAGCGGAUGAAGUGAUGCAACACUGGAGCCGCUGGGAACUAAUUUGUA UGCGAAAGUAUAUUGAUUAGUUUUGGAG-3'
L-16 preparation forward primer	5'-TAATACGACTCACTATAGGTTTGGAGGGAAAAGTTATCA-3'
L-16 preparation reverse primer	5'-/i2OMeC/i2OMeT/CCAAAACTAATCAATATACTTT-3'

Analytical Data of Compounds

Note*: The unknown impurity: Around 3.3 ppm (water peak),2.5 ppm (solvent peak) and 1.00 ppm –1.42 ppm in NMR are respectively from the DMSO and eluent.*

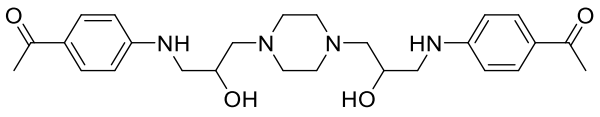

1,1'-(((piperazine-1,4-diylbis(2-hydroxypropane-3,1-diyl))bis(azanediyl))bis(4,1-phenylene))bis(ethan-1-one) (ZPT-084.1)

^{1}H NMR (400 MHz, DMSO) δ 7.90 – 7.48 (m, 4H), 6.79 – 6.35 (m, 6H), 4.75 (d, *J* = 4.3 Hz, 2H), 3.77 (s, 2H), 3.22 (dd, *J* = 11.5, 5.8 Hz, 2H), 3.11 – 2.93 (m, 2H), 2.62 – 2.05 (m, 18H).

^{13}C NMR (101 MHz, DMSO) δ 195.37, 153.60, 130.89, 125.11, 111.22, 66.84, 62.79, 54.14, 47.95, 26.33.

HRMS (ESI) calcd for $C_{26}H_{37}N_4O_4$ $(M+H)^+$: 469.2809, found: 469.2807.

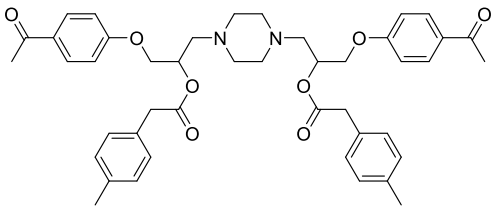

piperazine-1,4-diylbis(3-(4-acetylphenoxy)propane-1,2-diyl) bis(2-(p-tolyl)acetate) (ZPT-084.2)

^{1}H NMR (400 MHz, DMSO) δ 7.89 (d, *J* = 8.8 Hz, 4H), 7.11 (d, *J* = 8.0 Hz, 4H), 7.04 (d, *J* = 7.4 Hz, 4H), 6.98 (d, *J* = 8.8 Hz, 4H), 5.33 – 5.18 (m, 4H), 4.18 (ddd, *J* = 17.2, 11.0, 4.7 Hz, 4H), 3.54 (d, *J* = 19.7 Hz, 4H), 2.56 – 2.42 (m, 12H), 2.32 – 2.26 (m, 6H), 2.22 (s, *J* = 5.8 Hz, 6H).

^{13}C NMR (101 MHz, DMSO) δ 196.75, 171.18, 162.51, 136.26, 131.68, 130.93, 130.62, 129.73, 129.52, 129.30, 129.10, 114.85, 69.84, 68.45, 57.80, 53.59, 33.82, 32.19, 26.89, 25.79, 24.93, 21.08.

HRMS (ESI) calcd for $C_{44}H_{51}N_2O_8$ $(M+H)^+$: 735.3640, found: 735.3657

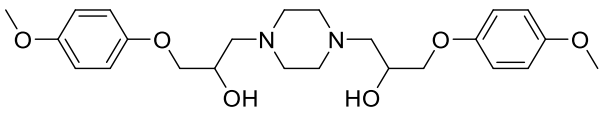

3,3'-(piperazine-1,4-diyl)bis(1-(4-methoxyphenoxy)propan-2-ol) (ZPT-084.3)

^{1}H NMR (400 MHz, DMSO) δ 6.99 – 6.56 (m, 8H), 4.69 (d, *J* = 4.4 Hz, 2H), 3.78 (dd, *J* = 13.0, 4.1 Hz, 4H), 3.72 – 3.65 (m, 2H), 3.58 (s, 6H), 2.45 – 2.38 (m, 2H), 2.33 – 2.19 (m, 10H).

HRMS (ESI) calcd for $C_{26}H_{37}N_4O_4$ $(M+H)^+$: 447.2495, found: 447.2498.

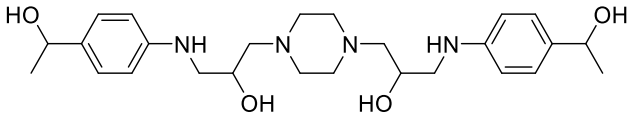

3,3'-(piperazine-1,4-diyl)bis(1-((4-(1-hydroxyethyl)phenyl)amino)propan-2-ol) (ZPT-084.4)

^{1}H NMR (400 MHz, DMSO) δ 7.04 (d, J = 8.4 Hz, 4H), 6.54 (d, J = 8.5 Hz, 4H), 5.34 (dd, J = 12.6, 7.4 Hz, 2H), 4.99 – 4.70 (m, 2H), 3.94 – 3.68 (m, 2H), 3.64 – 3.33 (m, 2H), 3.11 (dd, J = 12.8, 4.7 Hz, 2H), 2.95 (ddd, J = 15.9, 13.7, 6.8 Hz, 2H), 2.62 – 2.26 (m, 4H), 1.27 (d, J = 6.4 Hz, 6H).

^{13}C NMR (101 MHz, DMSO) δ 148.20, 135.00, 126.56, 112.16, 68.38, 66.64, 62.85, 53.78, 48.96, 45.92, 26.33.

HRMS (ESI) calcd for $C_{26}H_{41}N_4O_4$ $(M+H)^+$: 473.3122, found: 473.3118.

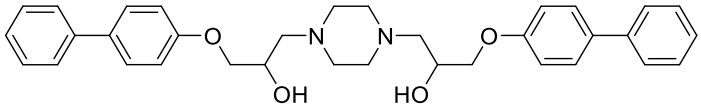

3,3'-(piperazine-1,4-diyl)bis(1-([1,1'-biphenyl]-4-yloxy)propan-2-ol) (ZPT-084.5)

^{1}H NMR (400 MHz, $CDCl_3$) δ 7.59 – 7.49 (m, 8H), 7.42 (dd, *J* = 10.5, 4.8 Hz, 4H), 7.31 (t, *J* = 6.8 Hz, 2H), 7.08 – 6.96 (m, 4H), 4.14 (td, *J* = 9.2, 4.6 Hz, 2H), 4.11 – 3.99 (m, 4H), 3.06 (s, 2H), 2.98 – 2.19 (m, 12H).

^{13}C NMR (101 MHz, $CDCl_3$) δ 158.28, 140.72, 134.13, 128.74, 128.17, 126.74, 114.85, 70.31, 65.59, 60.44.

HRMS (ESI) calcd for $C_{26}H_{37}N_4O_4$ $(M+H)^+$: 539.2910, found: 539.2915.

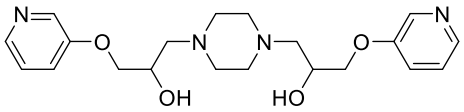

3,3'-(piperazine-1,4-diyl)bis(1-(pyridin-3-yloxy)propan-2-ol) (ZPT-084.6)

^{1}H NMR (400 MHz, DMSO) δ 8.14 (d, *J* = 2.8 Hz, 2H), 8.01 (d, *J* = 4.5 Hz, 2H), 7.27 – 7.22 (m, 2H), 7.17 (dd, *J* = 8.4, 4.6 Hz, 2H), 4.80 (s, 2H), 3.91 (d, *J* = 6.5 Hz, 2H), 3.86 – 3.73 (m, 4H), 2.46 – 2.11 (m, 12H).

HRMS (ESI) calcd for $C_{26}H_{37}N_4O_4$ $(M+H)^+$: 389.2189, found: 389.2193.

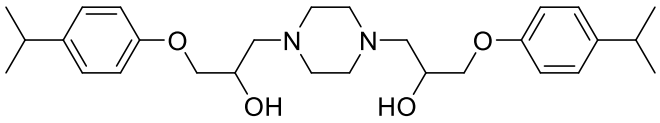

3,3'-(piperazine-1,4-diyl)bis(1-(4-isopropylphenoxy)propan-2-ol) (ZPT-084.7)

^{1}H NMR (400 MHz, DMSO-d_6) δ 7.10 (d, *J* = 8.1 Hz, 4H), 6.81 (d, *J* = 8.1 Hz, 4H), 4.91 – 4.45 (m, 2H), 3.89 (d, *J* = 8.0 Hz, 4H), 3.79 (d, *J* = 8.8 Hz, 2H), 2.79 (p, *J* = 7.0 Hz, 4H), 2.47-2.31 (m, 12H), 1.13 (d, *J* = 7.0 Hz, 12H).

HRMS (ESI) calcd for $C_{26}H_{37}N_4O_4$ $(M+H)^+$: 471.3223, found: 471.3228.

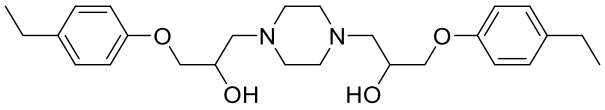

3,3'-(piperazine-1,4-diyl)bis(1-(4-ethylphenoxy)propan-2-ol) (ZPT-084.8)

^{1}H NMR (400 MHz, DMSO) δ 7.10 (d, *J* = 8.5 Hz, 4H), 6.84 (d, *J* = 8.5 Hz, 4H), 4.81 (d, *J* = 4.4 Hz, 2H), 3.99 – 3.90 (m, 4H), 3.81 (dd, *J* = 10.9, 7.3 Hz, 2H), 2.54 (d, *J* = 7.6 Hz, 2H), 2.51 (dd, *J* = 4.3, 2.5 Hz, 4H), 2.44 – 2.31 (m, 10H), 1.14 (t, *J* = 7.6 Hz, 6H).

HRMS (ESI) calcd for $C_{26}H_{37}N_4O_4$ $(M+H)^+$: 442.2832, found: 442.2834.

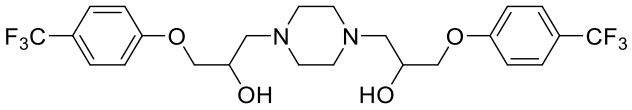

3,3'-(piperazine-1,4-diyl)bis(1-(4-(trifluoromethyl)phenoxy)propan-2-ol) (ZPT-084.9)

^{1}H NMR (400 MHz, DMSO) δ 7.59 (d, *J* = 8.6 Hz, 4H), 7.08 (d, *J* = 8.6 Hz, 4H), 4.86 (d, *J* = 2.3 Hz, 2H), 4.30 – 3.77 (m, 6H), 2.85 – 1.98 (m, 12H).

^{13}C NMR (101 MHz, DMSO) δ 162.12, 127.35 (d, *J* = 4.04 Hz), 125.06 (d, *J* = 272.7 Hz), 121.45 (d, *J* = 32.32 Hz), 121.01, 120.96, 120.54, 115.45, 71.90, 66.81, 61.36, 54.06.

^{19}F NMR (376 MHz, DMSO) δ -59.77, -59.78, -59.80, -59.81, -60.48, -60.52, -60.57, -60.61, -60.66, -60.71.

HRMS (ESI) calcd for $C_{24}H_{29}F_6N_2O_4$ $(M+H)^+$: 523.2026, found: 523.2024

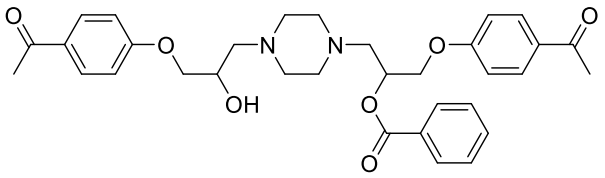

1-(4-acetylphenoxy)-3-(4-(3-(4-acetylphenoxy)-2-hydroxypropyl)piperazin-1-yl)propan-2-yl benzoate (ZPT-084.10)

^{1}H NMR (400 MHz, DMSO) δ 8.13 – 7.81 (m, 6H), 7.68 – 7.51 (m, 3H), 7.20 – 6.93 (m, 4H), 5.52 (d, *J* = 3.0 Hz, 1H), 4.39 (q, *J* = 11.2 Hz, 2H), 4.01 (dd, *J* = 36.0, 6.7 Hz, 3H), 2.92 – 2.26 (m, 18H).

^{13}C NMR (101 MHz, DMSO) δ 196.75, 165.70, 162.96, 162.60, 133.93, 130.96, 130.66, 130.35, 130.13, 129.71, 129.24, 114.96, 114.80, 71.50, 70.52, 68.53, 57.68, 57.65, 26.88.

HRMS (ESI) calcd for $C_{33}H_{39}N_2O_7$ $(M+H)^+$: 575.2752, found: 575.2747.

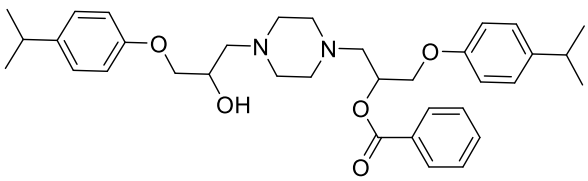

1-(4-(2-hydroxy-3-(4-isopropylphenoxy)propyl)piperazin-1-yl)-3-(4-isopropylphenoxy)propan-2-yl benzoate (ZPT-084.11)

^{1}H NMR (400 MHz, $CDCl_3$) δ 8.18 – 7.90 (m, 2H), 7.65 – 7.52 (m, 1H), 7.43 (dd, *J* = 10.6, 4.8 Hz, 2H), 7.13 (d, *J* = 8.6 Hz, 4H), 6.91 – 6.80 (m, 4H), 5.70 – 5.31 (m, 1H), 4.33 – 3.85 (m, 6H), 2.92 – 2.83 (m, 2H), 2.82 – 2.73 (m, 2H), 2.70 – 2.40 (m, 10H), 1.22 (d, *J* = 6.9 Hz, 12H).

^{13}C NMR (101 MHz, $CDCl_3$) δ 166.06, 156.80, 141.51, 141.39, 133.01, 130.24, 129.72, 128.35, 127.27, 127.24, 114.58, 114.37, 70.82, 70.33, 67.92, 65.53, 60.50, 58.01, 53.76, 53.38, 49.15, 33.98, 33.29, 25.64, 24.96, 24.21.

HRMS (ESI) calcd for $C_{35}H_{47}N_2O_5$ $(M+H)^+$: 575.3479, found: 575.3475

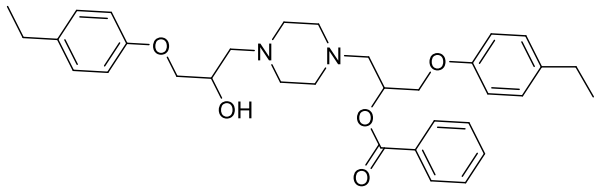

1-(4-ethylphenoxy)-3-(4-(3-(4-ethylphenoxy)-2-hydroxypropyl)piperazin-1-yl)propan-2-yl benzoate (ZPT-084.12)

^{1}H NMR (400 MHz, DMSO-d_6) δ 7.90 (d, *J* = 7.4 Hz, 2H), 7.61 (d, *J* = 7.3 Hz, 1H), 7.48 (t, *J* = 7.6 Hz, 2H), 7.12 – 6.99 (m, 4H), 6.81 (dd, *J* = 16.4, 8.2 Hz, 4H), 5.43 (dd, *J* = 6.1, 3.8 Hz, 1H), 4.74 (d, *J* = 4.4 Hz, 1H), 4.27 – 4.12 (m, 2H), 3.87 (d, *J* = 7.7 Hz, 2H), 3.80 – 3.71 (m, 1H), 2.65 (d, *J* = 6.3 Hz, 2H), 2.54 – 2.45 (m, 4H), 2.43-2.24 (m, 10H), 1.09 (td, *J* = 7.5, 2.9 Hz, 6H).

HRMS (ESI) calcd for $C_{26}H_{37}N_4O_4$ $(M+H)^+$: 546.3094, found: 546.3096.

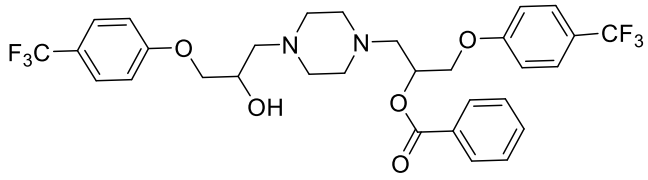

1-(4-(2-hydroxy-3-(4-(trifluoromethyl)phenoxy)propyl)piperazin-1-yl)-3-(4-(trifluoromethyl)phenoxy)propan-2-yl benzoate (ZPT-084.13)

^{1}H NMR (400 MHz, DMSO) δ 7.90 (d, *J* = 7.2 Hz, 2H), 7.60 (d, *J* = 7.1 Hz, 5H), 7.48 (t, *J* = 7.2 Hz, 2H), 7.10 (dd, *J* = 18.0, 8.1 Hz, 4H), 5.80 – 5.39 (m, 1H), 4.85 (s, 1H), 4.35 (s, 2H), 4.20 – 3.81 (m, 3H), 2.68 – 2.67 (m, 2H), 2.47 – 2.32 (m, 10H).

^{13}C NMR (101 MHz, DMSO) δ 165.66, 162.11, 161.66, 132.02(d, *J* =285.83 Hz), 129.44 (d, *J* = 47.47 Hz), 127.51, 127.48, 127.44, 127.41, 127.37, 127.33, 126.37, 126.34, 126.30, 123.71, 123.63, 123.61, 123.58, 122.08, 122.03, 121.58, 121.27, 115.58 (d, *J* = 21.21 Hz), 71.88, 70.60, 68.65, 66.79, 61.29, 57.92, 54.02, 53.76, 47.97, 33.82, 25.79, 24.92.

^{19}F NMR (376 MHz, DMSO) δ -59.55, -59.78, -59.88, -60.27, -60.37, -60.49, -60.58, -60.70, -60.79.

HRMS (ESI) calcd for $C_{31}H_{33}F_6N_2O_5$ $(M+H)^+$: 627.2288, found: 627.2286

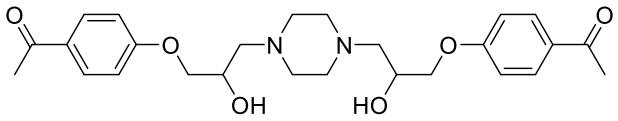

1,1'-(((piperazine-1,4-diylbis(2-hydroxypropane-3,1-diyl))bis(oxy))bis(4,1-phenylene))bis(ethan-1-one) (ZPT-084.14)

^{1}H NMR (400 MHz, DMSO) δ 7.92 (d, *J* = 8.5 Hz, 4H), 7.04 (d, *J* = 8.5 Hz, 4H), 4.91 (d, *J* = 3.2 Hz, 2H), 4.07 (t, *J* = 6.2 Hz, 2H), 3.95 (d, *J* = 7.3 Hz, 4H), 2.66 – 2.26 (m, 18H).

HRMS (ESI) calcd for $C_{26}H_{37}N_4O_4$ $(M+H)^+$: 471.2495, found: 471.2496.

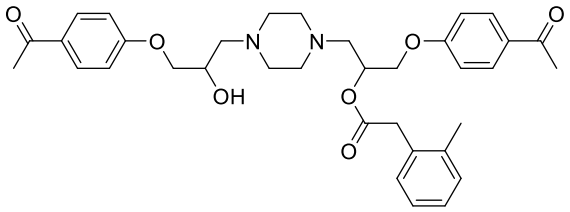

1-(4-acetylphenoxy)-3-(4-(3-(4-acetylphenoxy)-2-hydroxypropyl)piperazin-1-yl)propan-2-yl 2-(o-tolyl)acetate (ZPT-084.15)

^{1}H NMR (400 MHz, DMSO) δ 8.10 – 7.80 (m, 6H), 7.66 – 7.48 (m, 3H), 7.26 – 6.88 (m, 3H), 5.54 (d, *J* = 2.4 Hz, 1H), 4.35 (q, *J* = 9.6 Hz, 2H), 4.13 (m, 3H), 3.51 (d, *J* = 16.6 Hz, 2H), 2.92 – 2.26 (m, 18H), 2.18 (s, 3H).

HRMS (ESI) calcd for $C_{26}H_{37}N_4O_4$ $(M+H)^+$: 602.2992, found: 602.2996.

Supplementary Movie 1 | ZPT-084 binds to L-16 allesteric binding site to induce large conformational changes to translocate the catalytic site away from the 5'-SS to inhibit catalysis.

Supplementary Data 1 | Information of compounds used in SHAP analysis, including 10,000 randomly sampled from 13 million commercial library, 5,000 randomly sampled from the CSTAR library, 994 compounds from the positive dataset, 3,767 compounds from the negative dataset, and 1,615 FDA-approved drugs.

Supplementary Data 2 | Information of 125 purchased compounds.